ELSEVIER

Polymer 41 (2000) 6851–6863

polymer

# Crosslinked polydimethylsiloxane exposed to oxygen plasma studied by neutron reflectometry and other surface specific techniques

H. Hillborg[a,b], J.F. Ankner[c], U.W. Gedde[a,*], G.D. Smith[d], H.K. Yasuda[e], K. Wikström[a]

[a]*Department of Polymer Technology, Royal Institute of Technology, SE-100 44 Stockholm, Sweden*
[b]*ABB Corporate Research, Department of High Voltage Engineering, SE-721 78 Västerås, Sweden*
[c]*Reactor Research Facility, University of Missouri-Columbia, Columbia, MO 65211, USA*
[d]*Department of Materials Science and Engineering and Department of Chemical and Fuels Engineering, University of Utah, Salt Lake City, UT 84 112, USA*
[e]*Center for Surface Science and Plasma Technology and Department of Chemical Engineering, University of Missouri-Columbia, Columbia, MO 65211, USA*

Received 16 August 1999; received in revised form 9 December 1999; accepted 10 January 2000

**Abstract**

Spin-coated specimens of crosslinked polydimethylsiloxane (PDMS) exposed to radio-frequency (RF) and microwave (MW) oxygen plasma were studied by specular neutron reflectometry, X-ray photoelectron spectroscopy (XPS), Wilhelmy balance, contact angle measurements, scanning electron microscopy and atomic force microscopy. Neutron reflectometry and XPS showed that the oxygen plasma led to the formation of a smooth (<10 nm), oxidised surface layer with a thickness of 130–160 nm. The oxidised layer contained a mixture of the original polymer and silicon bonded to three or four oxygen atoms ($SiO_x$). The oxidised layer was thinner after longer plasma exposure, indicating a decrease in specific volume due to a conversion of the polymer structure to an inorganic $SiO_x$-rich structure. The formation of the $SiO_x$-containing layer with low segmental mobility was further confirmed by the small hysteresis in the Wilhelmy balance measurements. The similarity in the hydrophobicity recovery kinetics of specimens aged in dry air, dry argon and vacuum and XPS data showed that the hydrophobicity recovery is not due to contamination through adsorption from the atmosphere but due to migration of low molar mass PDMS species to the surface. Scanning electron microscopy also showed the presence of surface cracks in heavily oxidised specimens. 

*Keywords*: Oxygen plasma; Polydimethylsiloxane; Surface properties

## 1. Introduction

Silicone rubbers are used as housing materials in outdoor high-voltage composite insulations, replacing the traditional porcelain insulation [1,2]. The polymer used in these rubbers is mostly polydimethylsiloxane (PDMS). The hydrophobicity of silicone rubbers provides a high surface resistivity and water repellence even in the presence of moisture and contaminants. The initially hydrophobic surface becomes progressively more hydrophilic after extensive exposure to electrical discharges [1,2] and it then loses its water repellence. This leads to wetting of the PDMS surface and trails of water can eventually lead to breakdown of the insulation. Exposure to oxygen plasma also causes a loss of hydrophobicity of PDMS [1,3] and this can be used as an accelerated method to simulate ageing. The original hydrophobicity is regained after several hours in the absence of electrical activity [1,2,4–8]. The ability to recover hydrophobicity is a very important property of silicone rubbers. Because of this much work has been done to reveal the underlying mechanisms. It has been suggested that external contamination of the polymer surface, transport of low molar mass PDMS species from the bulk to the surface, chain scission, and reorientation of polar species from the surface into the bulk are the responsible mechanisms [3,7–9]. Exposure of PDMS to corona discharges or oxygen plasma leads not only to oxidation and chain scission but also to crosslinking and the formation of an inorganic silica-like surface layer [3,10], which retards the recovery of hydrophobicity [11]. This oxidised layer consists partly of $SiO_x$, i.e. silicon bonded to three or four oxygen atoms.

This paper presents data obtained by specular neutron reflectometry together with a range of other surface assessment methods on oxygen-plasma-exposed silicone rubber specimens prepared by spin coating. Neutron reflectometry is a powerful tool for the investigation of the surface

* Corresponding author. Tel.: + 46-8-7907640; fax: + 46-8-7906946.
*E-mail address:* gedde@polymer.kth.se (U.W. Gedde).

0032-3861/00/$ - see front matter 
PII: S0032-3861(00)00039-2

behaviour of polymers under atmospheric conditions. The incident neutrons interact with the nucleus in the core of the atoms via nuclear forces, detecting variations in scattering length density as a function of depth into the specimen. The method is non-destructive [12]. The technique provides sub-nanometre resolution with penetration depths of hundreds of nanometres. Typical applications of neutron reflectivity are investigations of polymer interdiffusion processes across interfaces [13–15]. Neutron reflectometry and X-ray photoelectron spectroscopy (XPS) confirmed the formation of an oxidised, $SiO_x$-rich surface layer in the specimens exposed to oxygen plasma. Information about the thickness and the chemical composition of the oxidised surface layer is presented. The surface topography was assessed using scanning electron microscopy and atomic force microscopy. The question about the origin of the hydrophobic recovery was addressed by studying oxygen-plasma-treated specimens aged in different atmospheres: dry air, argon and vacuum. The similarity in the hydrophobic recovery kinetics of the specimens exposed to these different atmospheres supported the view that hydrophobic recovery is not due to contamination through adsorption from the atmosphere but due to migration of PDMS or its oligomers to the surface. This was also substantiated by XPS. Hydrophobic recovery as revealed by contact angle measurements and by the Wilhelmy balance technique indicated that the segmental mobility of the molecules in the surface layer decreased on the exposure to oxygen plasma.

## 2. Experimental

### 2.1. Specimen preparation

A vinyldimethyl-terminated polydimethylsiloxane ($\bar{M}_w = 31\,400$ g mol$^{-1}$; $\bar{M}_w/\bar{M}_n = 1.94$, determined by size exclusion chromatography using PDMS standards for calibration. The solvent used was $CHCl_3$) was crosslinked in a hydrosilylation reaction, using a (30–35%) methylhydro-(65–70%) dimethylsiloxane copolymer ($\bar{M}_w =$ 2100 g mol$^{-1}$) as crosslinker. The ratio of hydride to vinyl groups was 2:1. A platinum divinyltetramethyl disiloxane complex was used as a catalyst at a concentration of 6 ppm. The chemicals were purchased from United Chemical Technologies Inc., USA, and were used as received. The reactants were diluted in heptane (Merck, >99% purity) to a 5 wt.% solution. The solution was filtered through a filter with a pore size of 0.45 μm and spin-coated onto silicon wafers at 3000 rpm where it was allowed to spin + dry over a period of 30 s. The silicon wafers were cleaned with ethanol and acetone before spin coating. The specimens were subsequently cured in a dust-free hood at 130°C for 4 h. The thickness of the films was in the order of 200 ± 30 nm according to ellipsometry.

Additional films with a thickness of 1 mm based on the same compound, for use in the Wilhelmy balance measurements were compression moulded. A Schwabenthan Polystat 400S compression moulding apparatus was used and the mouldings were performed at 160°C and 6 MPa pressure for 20 min and thereafter post-cured at 170°C for more than 3 h.

### 2.2. Plasma treatment and ageing conditions after plasma exposure

Specimens analysed by neutron reflectometry, Wilhelmy balance, contact angle measurements, atomic force microscopy and scanning electron microscopy were exposed to oxygen plasma in a bell-jar reactor, type LCD-1200-400A from Shimadzu, Japan, with a volume of approximately $75 \times 10^{-3}$ m$^3$. Treatments were performed at a pressure of 26.6 Pa of ultra-pure oxygen (Scotts Special Gases Inc., USA) and a gas flow rate of $4.37 \times 10^{-6}$ m$^3$ s$^{-1}$. The frequency was 13.56 MHz and the power was 40 W. The disc was rotated in order to achieve a uniform plasma exposure of the specimens. This treatment hereafter referred to as radio-frequency (RF) oxygen plasma treatment.

Specimens analysed by contact angle measurements, XPS, atomic force microscopy and scanning electron microscopy were exposed to oxygen plasma in a V15-G microwave frequency reactor from Plasma-Finish GmbH, Germany. The treatments were performed at 27.0 Pa of ultra-pure oxygen (AGA, Sweden) and a gas flow of $8.3 \times 10^{-7}$ m$^3$ s$^{-1}$. The frequency was 2.45 GHz and the power was 40 W. This method is referred to as microwave (MW) oxygen plasma treatment.

A few specimens later analysed by scanning electron microscopy were subjected to corona discharges in dry air (pressure 100 kPa) using a set-up described by Hillborg and Gedde [11]. The applied 50 Hz AC voltage was 20 kV (peak value) between the 87 mm (diameter) electrode with 31 needle electrodes and the ground plate. The distance between the tips of the lowest needles and the electrode ground plate was 40 mm. The integrated corona charge transfer was 2.6 W.

The specimens were aged in dry air at room temperature after exposure to oxygen plasma or corona discharges for different periods of time before performing the various surface analyses. Some specimens were also aged under vacuum or in argon (extra pure quality) at room temperature.

### 2.3. Neutron reflectometry

The neutron scattering experiments on spin-coated specimens were performed at the Missouri University Research Reactor (MURR), University of Missouri-Columbia, USA. This instrument featured a monochromatic beam ($\lambda =$ 0.235 nm) used in an angle-dispersive configuration with a single $^3$He detector [16]. Data collection required a total time of 4 h, which included a quasi-specular scan that was later subtracted from the raw specular data as a background correction. The reflected intensity data, normalised to unit

incident intensity were measured as a function of the change in neutron momentum transfer normal to the surface ($Q = (4\pi/\lambda)\sin\theta$, where $\lambda$ is the wavelength of the incident neutron beam and $\theta$ is the incident angle). The coherent scattering length ($b_{mon}$) was calculated using the repeating unit of the polymer according to:

$$b_{mon} = \sum_i x_i b_i \quad (1)$$

where $x_i$ is the number of atoms of element $i$ and $b_i$ are the coherent scattering lengths of the individual atoms of the repeating unit. The coherent scattering length values of the different elements considered were 6.6460 fm (carbon), 4.1491 fm (silicon), 5.803 fm (oxygen) and −3.7390 fm (hydrogen) [17]. The coherent scattering length of PDMS ($b_{PDMS}$) was calculated according to:

$$b_{PDMS} = 2b_C + b_{Si} + b_O + 6b_H \quad (2)$$

where $b_C$, $b_{Si}$, $b_O$ and $b_H$ are the coherent scattering lengths of carbon, silicon, oxygen and hydrogen, respectively. Application of Eq. (2) to the scattering length data for the appropriate elements yields a value for $b_{PDMS}$ of 0.810 fm. The atoms in the crosslinks were neglected in this calculation. The specimen structures are expressed by the scattering length density ($nb$) at the critical angle for total external reflection ($Q_c$) of the layers comprising the films and is expressed as [18]:

$$nb = \frac{Q_c^2}{16\pi} \quad (3)$$

where $n$ is the number density of repeating units, which is given by:

$$n = \frac{\rho N_A}{M} \quad (4)$$

where $\rho$ is the density, $N_A$ is the Avogadro number ($6.02 \times 10^{23}$ mol$^{-1}$) and $M$ is the molar mass of the repeating unit. The profile of the scattering length density as a function of layer depth ($z$) was varied to fit the experimental data using an asymmetric interfacial width error function. The principles of neutron reflectivity and the analysis can be found elsewhere [12,18,19].

Fig. 1 shows a schematic figure of a spin-coated specimen after exposure to oxygen plasma and the spatial parameters that characterise the layer structures.

### 2.4. Contact angle measurements

Dynamic contact angle measurements were performed on spin-coated specimens using a Ramé Hart goniometer using the sessile drop technique [20]. Deionized water (18.4 MΩ cm) was used. Each data point given is based on 10 contact angle measurements at five different positions on the specimen. Advancing and receding contact angles were measured with the needle remaining in the water droplet.

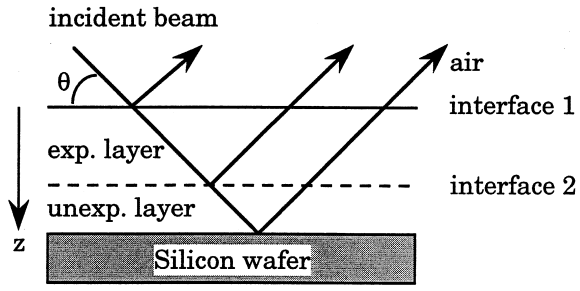


Fig. 1. Schematic figure of a spin-coated PDMS film onto a silicon wafer after plasma exposure showing oxidised and unoxidised layers. The angle of incidence ($\theta$) of neutrons is shown.

### 2.5. Wilhelmy balance

The dynamic contact angle was measured by a fully computer-controlled, automated tensiometer Sigma 70 (KSV Instruments, Finland). The measured force ($F$) acting on a thin plate partially immersed in a liquid can be represented by the force balance equation [21]:

$$F = \rho g t H d + L\gamma_L \cos\phi \quad (5)$$

where $\rho$ is the density of the liquid, $g$ is the gravitational acceleration, $t$ is the thickness of the plate (1.0 mm), $H$ is the width of the plate (3.5–3.7 mm), $d$ is the immersion depth, $L$ is the perimeter of the plate, i.e. $2(t + H)$, $\gamma_L$ is the liquid surface tension and $\phi$ is the dynamic contact angle at the three-phase line (the liquid–vapour interface at the surface of the moving specimen). The first term is the buoyancy force and the second term is the force that originates from the interfacial interaction. The balance was set to zero before or after measurement, so that the measured force ($F$) did not include the gravitational force, $mg$. The surface tension of water was measured to be 73 mN m$^{-1}$ by the Du Nouy ring method [22]. Distilled and deionised water was poured into a beaker and placed inside a closed test chamber together with the specimen, to minimise pollution from the air. The speed of immersion and withdrawal was 5 mm min$^{-1}$.

In the first cycle the specimen was first immersed to a depth of 10 mm (A–B–C in Fig. 2), and withdrawn to a depth of 5 mm (C–D–E). In cycle 2, the specimen was

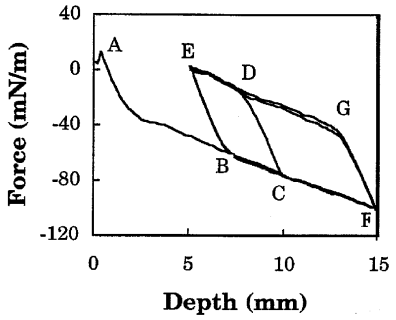


Fig. 2. The measured force ($F$) in the Wilhelmy balance as a function of immersion depth in water recorded for an unexposed specimen.

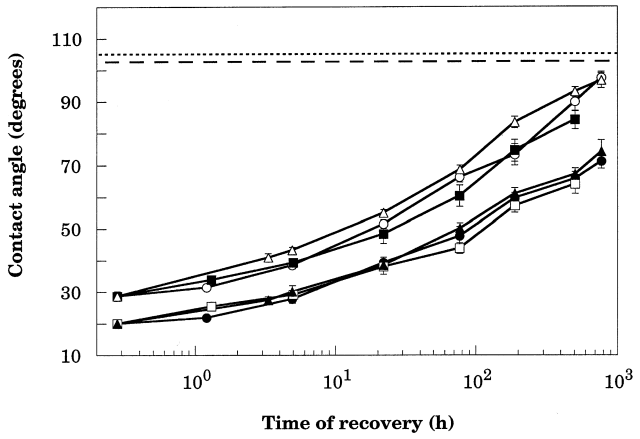


Fig. 3. Contact angle as a function of the ageing time at room temperature of specimen exposed to 80 s of MW oxygen plasma followed by ageing in different atmospheres: advancing angle, dry air (○); receding angle, dry air (●); advancing angle, argon (■); receding angle, argon (□); advancing angle, vacuum (△); receding angle, vacuum (▲). The error bars indicate a 90% confidence interval. Initial contact angles: advancing (- - -) and receding (– – –).

immersed further to a depth of 15 mm (E–B–F) and withdrawn to 5 mm (F–G–E). In cycle 3, the same pattern of immersion and withdrawal as cycle 2 was repeated (E–B–F–G–E). Measurements were performed on 1 mm thick specimens, immediately, 24, 144 and 288 h after the oxygen plasma exposure. Each individual specimen was used for one measurement only.

### 2.6. X-ray photoelectron spectroscopy

Spin-coated specimens were analysed by XPS before and after oxygen plasma exposure. Plasma-treated spin-coated specimens were also analysed after ageing in dry air at room temperature. Before the XPS analyses the specimens were degassed in vacuum. The XPS spectra were obtained using an AXIS-HS spectrometer from Kratos Analytical. The monochromatic Al $K_\alpha$ radiation used was operated at 15 kV and 300 W. The pressure in the sample chamber was between $5 \times 10^{-6}$ and $1 \times 10^{-5}$ Pa. Survey spectra were recorded at an 80 eV pass energy and the high resolution spectra of the Si 2p peak at 20 eV pass energy. The spectra were referenced to the O1s-line (binding energy = 532.0 eV). A low-energy electron flood gun was used to neutralise sample charging.

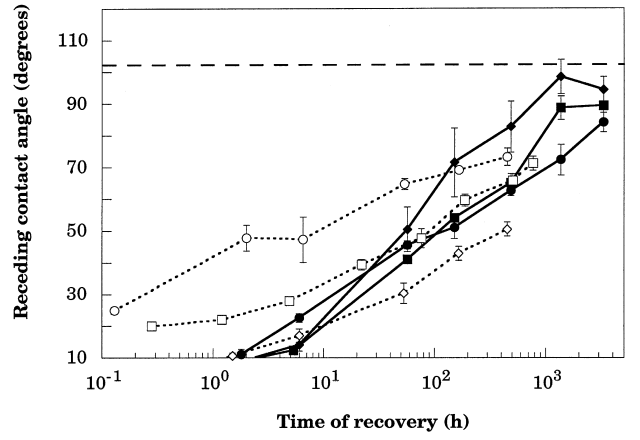


Fig. 4. Receding contact angle for specimen exposed to oxygen plasma for different periods of time as a function of ageing time in dry air at room temperature after the plasma treatment: 30 s of RF plasma (●); 80 s of RF plasma (■); 180 s of RF plasma (◆); 30 s of MW plasma (○); 80 s of MW plasma (□); 180 s of MW plasma (◇). The error bars indicate a 90% confidence interval.

### 2.7. Atomic force microscopy and scanning electron microscopy

The surface structure of spin-coated specimens (unexposed and after exposure to oxygen plasma and corona discharges) were studied in an atomic force microscope utilising the tapping mode (Nanoscope IIIA Multimode Atomic Force Microscope) and a Jeol JSM-5400 scanning electron microscope. Specimens examined in the scanning electron microscope were coated with Au/Pd (60:40) before examination, using a Desk II from Denton Vacuum, operated at 45 mA for 30 s.

## 3. Results and discussion

### 3.1. Influence of ageing atmosphere

Fig. 3 shows the advancing and receding contact angles as functions of ageing time of specimens exposed to 80 s of MW oxygen plasma followed by ageing in different atmospheres: dry air, argon and vacuum. The hydrophobicity recovery rates as revealed by the contact angles were essentially identical within error, for ageing in all three atmospheres. The recovery of hydrophobicity of the specimen aged in vacuum as assessed by the advancing contact angle was, however, slightly faster during the first 200 h. The initial advancing (105°) and receding (102°C) are shown as dotted lines in Fig. 3. Complete hydrophobic recovery was not achieved during the time period of the experiment.

The similarity in hydrophobic recovery of the specimens aged in different surroundings (dry air, argon and vacuum) strongly suggests that the hydrophobicity recovery was not due to contamination through adsorption from the surrounding atmosphere. This is in accordance with data of Owen et al. [23] who excluded atmosphere contamination as a possible explanation for hydrophobic recovery after performing studies of hydrophobic recovery of PDMS in a clean room environment after exposure to corona discharges. The reason for the slightly more rapid increase in the advancing contact angle for the specimen aged in vacuum remains unknown but this finding is inconsistent with the idea of hydrophobic recovery by adsorption from the atmosphere.

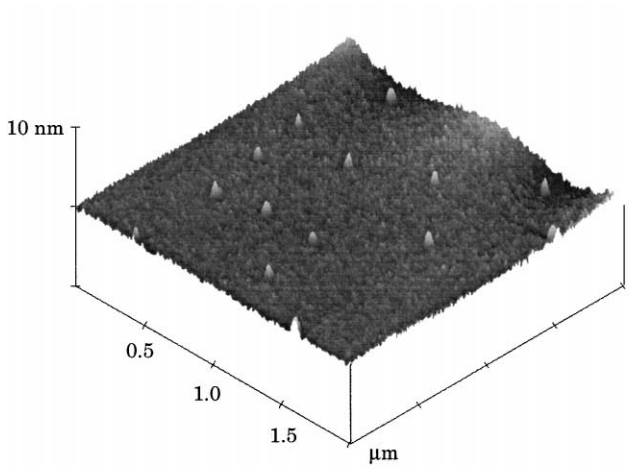


(a)

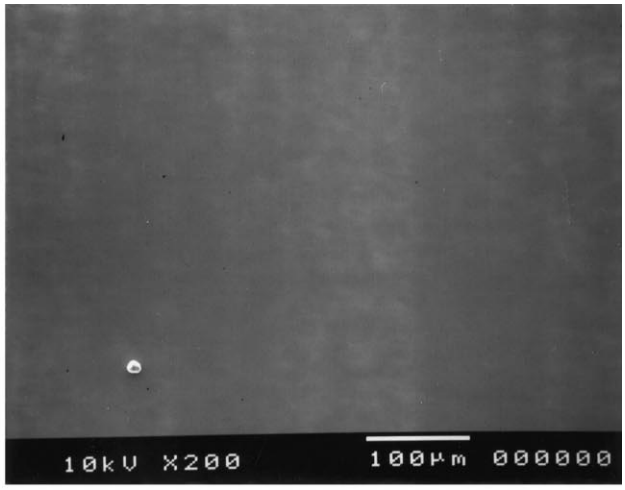


(b)

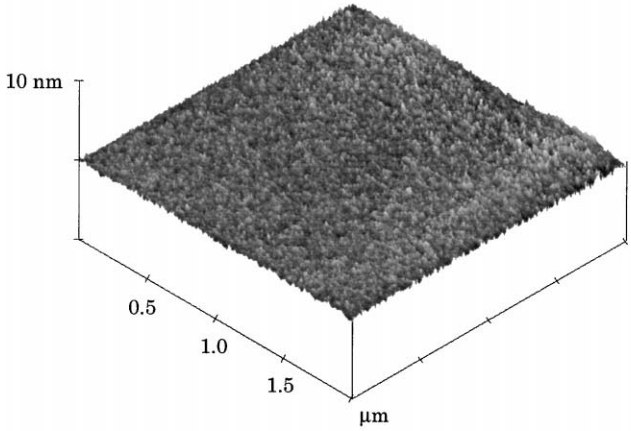


(c)

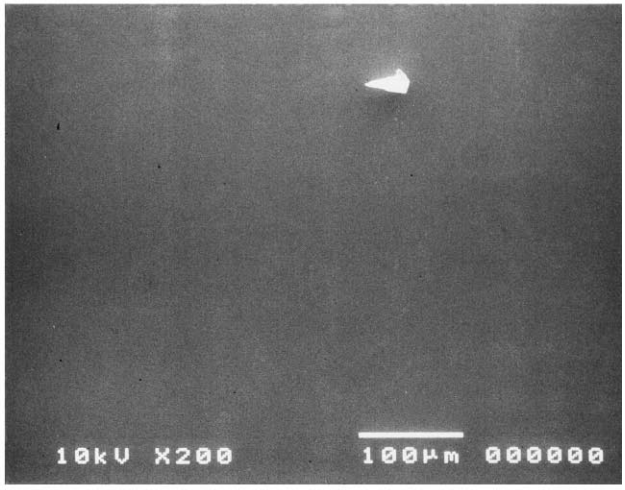


(d)

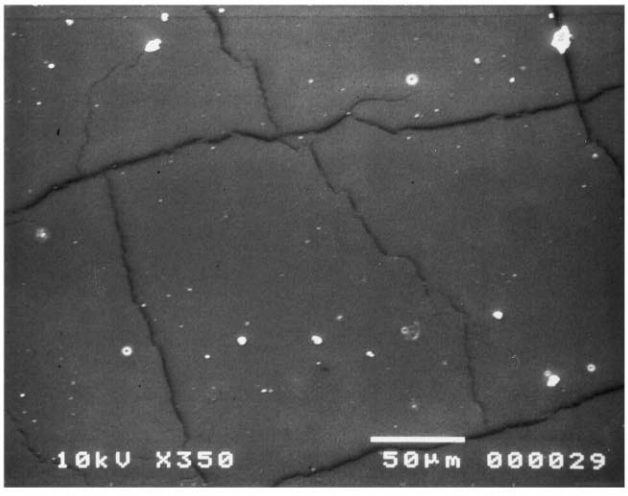


(e)

Fig. 5. Scanning electron micrographs and atomic force micrographs of plasma treated specimen: (a) 180 s of MW oxygen plasma (AFM); (b) 180 s of MW oxygen plasma (SEM); (c) 180 s of RF oxygen plasma (AFM); (d) 180 s of RF oxygen plasma (SEM); (e) Corona discharge for 3 h (SEM).

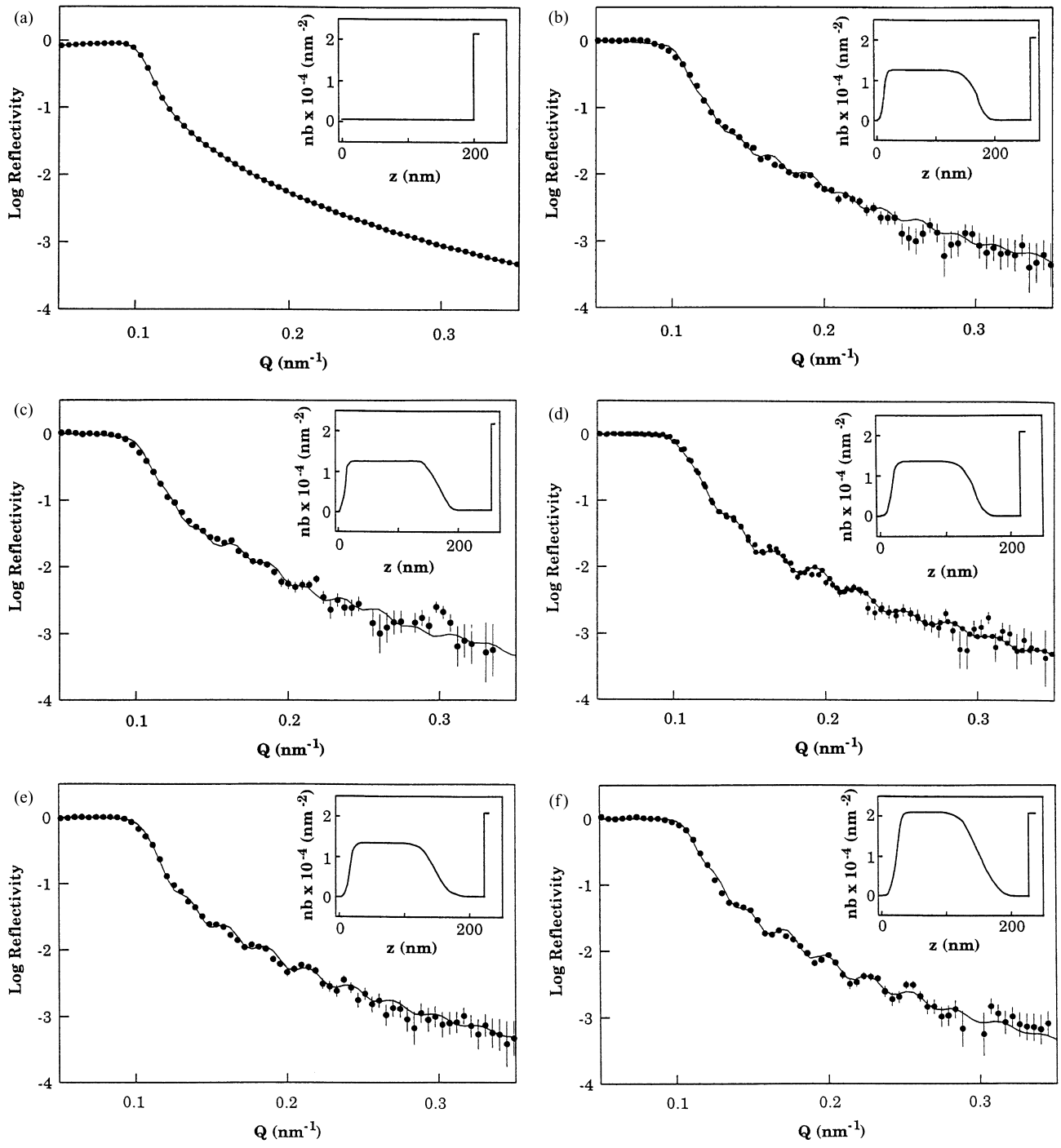


Fig. 6. Neutron reflectivity as a function of the scattering vector ($Q = (4\pi/\lambda) \sin \theta$). The inset figures show the profile of scattering length density (*nb*) as a function of the layer depth (*z*). The continuous lines displayed in figures a–f, show the best fits to the experimental data: (a) unexposed specimen; (b) specimen aged for 144 h after 80 s of RF oxygen plasma; (c) specimen aged for 288 h after 80 s of RF oxygen plasma; (d) specimen directly after 180 s of RF oxygen plasma; (e) specimen aged for 144 h after 180 s of RF oxygen plasma; (f) specimen aged for 288 h after 180 s of RF oxygen plasma; (g) specimen directly after 180 s RF oxygen plasma; the continuous line was calculated assuming a uniformly oxidised PDMS layer; (h) specimen directly after 180 s of RF oxygen plasma; the continuous lines were calculated using the following thickness values for the oxidised layer: 110 nm (- - -) and 160 nm (—).

### *3.2. Hydrophobicity recovery of specimens exposed to different oxygen plasma treatments*

Fig. 4 shows the receding contact angle as a function of the recovery time after exposure to RF and MW oxygen plasma. Specimens subjected to the RF plasma initially showed a very low receding contact angle, essentially independent of the plasma exposure time (30–180 s), and a subsequent, relatively rapid, recovery of hydrophobicity. The hydrophobic recovery was faster for specimens exposed

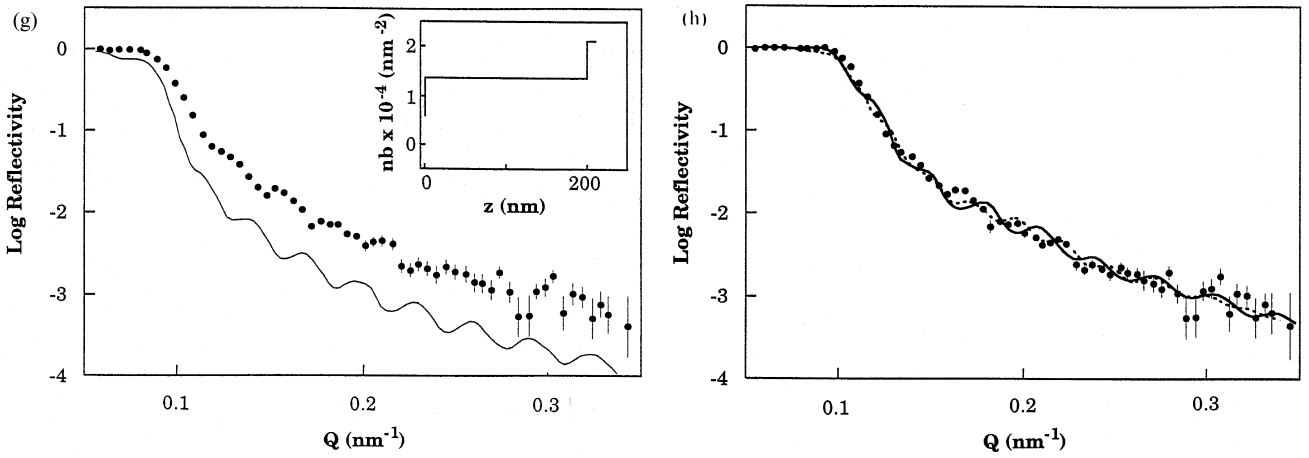


Fig. 6. (*continued*)

to a higher RF plasma dose (plasma treatment time). The time to reach almost full original hydrophobicity (~95° receding contact angle) decreased from approximately 10 000 h (30 s plasma exposure) to 1000 h (180 s plasma exposure). The hydrophobic recovery kinetics of specimens exposed to corona discharges were reported in an earlier paper [11] and the data showed basically a similar trend as for the specimens exposed to the RF oxygen plasma. The recovery time was ~1000 h after short-term exposure to the corona discharges (0.3 and 1 h), whereas a specimen exposed to corona during 200 h showed full recovery after only 200 h [11]. By bending of specimens exposed to an extended corona treatment, the recovery time was shortened even further to 8–9 h [11].

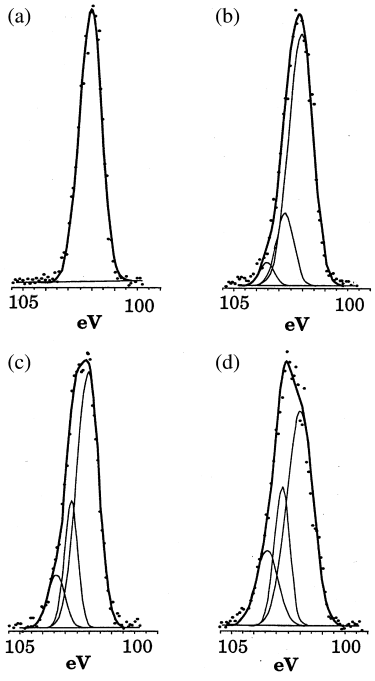


Fig. 7. Curve resolution of the Si 2p peak of spin-coated specimen exposed to MW oxygen plasma for: (a) 0 s; (b) 30 s; (c) 80 s; (d) 180 s. The plasma-exposed specimens had been aged in dry air at 23°C for 260 h. The Si 2p peak was resolved into three peaks located at 102.1, 102.8 and 103.4 eV, respectively.

The specimens exposed to the MW oxygen plasma showed a decrease in receding contact angle with increasing plasma dose immediately after the plasma exposure (Fig. 4). The hydrophobic recovery rate decreased with increasing plasma exposure time and particularly the specimen exposed to the longest plasma exposure time (180 s) showed a very slow hydrophobic recovery.

Fig. 5 presents AFM and SEM micrographs of specimens exposed to RF and MW oxygen plasma and corona discharges. The specimens exposed to 180 s of oxygen plasma (both RF and MW plasmas) were very smooth, with a roughness of less than 10 nm and without signs of surface cracks (Fig. 5a–d). The unexposed specimens showed a similar surface texture according to SEM (The unexposed specimens could not be analysed by AFM due to interference between the soft surface and the tip of the cantilever). It can be concluded that the oxygen plasma treatments caused no detectable change in the surface roughness. The specimens exposed to extensive corona discharges (3 h exposure) showed a very smooth surface with occasional surface cracks (Fig. 5e). It should be noted that these specimen were subjected to minor deformations by the preparation procedure prior to the SEM studies.

It is shown in Sections 3.3–3.6 that a thin, oxidised surface layer is formed on the specimens exposed to oxygen plasma. XPS data (Fig. 7) showed that a significant proportion of the oxidised layer contained silicon bonded to 3 or 4 oxygen atoms ($SiO_x$). The degree of conversion of organic to inorganic silicon ($SiO_x$) increased with increasing MW plasma dose (Fig. 7 and Table 3). A similar result was reported for samples exposed to corona discharges [11]. It may be assumed that samples exposed to RF plasma also would develop an oxidised surface layer with a gradually increasing proportion of $SiO_x$ with increasing plasma exposure time. The available free volume for diffusion of low molar mass species, tentatively the suggested mechanism

for the hydrophobic recovery, is greatly reduced in the denser, oxidised top layer. A continuous $SiO_x$ layer would reduce the migration rate of low molar mass PDMS from the bulk to the surface and hence reduce the hydrophobicity recovery rate. The specimens exposed to the MW oxygen plasma thus behave in accordance with this scheme. The decrease in the hydrophobic recovery rate with increasing MW plasma dose is thus due to gradual densification of the oxidised layer.

The fast hydrophobic recovery of the specimens exposed to extended corona can be explained by the finding of Fritz and Owen [24] that heavily oxidised layers show cracks. Indeed, SEM revealed similar cracks on the specimen exposed to extensive corona (Fig. 5e). The formation of a surface layer rich in $SiO_x$ involves a significant reduction in specific volume. This volume change leads to a build-up of tensile stresses in the film plane and the formation of surface cracks. Fritz and Owen [24] reported the dose of oxygen plasma required to produce cracking to 25 W during 10 min at an oxygen pressure of 70 Pa. The surface cracks permit fast hydrophobic recovery by rapid pore diffusion of low molar mass species and the increase in hydrophobic recovery rate with increasing corona dose can be fully explained by this scheme.

The specimens exposed to the RF plasma showed an increase in the hydrophobic recovery rate with increasing plasma exposure time (Fig. 4). This finding would suggest that the oxidised surface layer was cracked. However, no surface cracks were detected by AFM and SEM in these specimens (Fig. 5). Another important aspect, not studied here but in a parallel work [25], concerns the nature of the migrating species. The important question is whether the mobile species are the same, independent of plasma (corona) dose or if there is a systematic change in their structure with plasma (corona) dose. GPC and GC/MS showed that the extractable species of samples exposed to corona consisted of two greatly different fractions: high molar mass ($M \approx 40\,000$–$100\,000$ g mol$^{-1}$) and low molar mass, mainly cyclic ($M \approx 300$–$600$ g mol$^{-1}$) products [25]. It was interesting to find that the proportion of the low molar mass cyclic species increased with increasing exposure time [25]. The lowering of the molar mass of the mobile species with increasing exposure time would lead to faster recovery of the hydrophobicity if it is assumed that the phase in which the small molecules diffuse is invariant or only changed moderately. The diffusivity ($D$) of unentangled PDMS in crosslinked PDMS scales with molar mass ($M$) of the diffusing species according to $D \propto M^{-0.8}$ [26]. This equation implies a difference in diffusivity between the low and high molar mass species by two orders of magnitude in an unoxidised PDMS network. The difference may even be larger in a more constrained $SiO_x$-rich phase.

The obtained results may be rationalised as follows: Exposure to plasma causes the formation of an oxidised surface layer containing dense $SiO_x$-rich material. The proportion of $SiO_x$ in the oxidised layer increases with increasing exposure time and hence the available free volume for diffusion of mobile (low molar mass) species decreases gradually. Cracking of the oxidised layer may occur spontaneously provided that the conversion of the organic material to $SiO_x$ is sufficiently. The plasma also causes degradation of the polymer network. The amount of mobile, low molar mass species increases with plasma exposure time and the molar mass of the mobile species decreases with increasing exposure time. The access to a large amount of very mobile cyclic molecules in specimens subjected to prolonged exposure to plasma promotes fast recovery of hydrophobicity. The results indicate that the balance between the two counteracting processes—the formation of a dense $SiO_x$-rich layer and the formation of very mobile, cyclic species—is sensitive to the type of plasma used.

### 3.3. Neutron reflectometry: chemical composition of oxidised surface layer

Fig. 6a shows the neutron reflectivity ($R$) as a function of neutron momentum transfer normal to the surface ($Q$) for unexposed spin-coated PDMS, where only the silicon wafer was detected. The scattering length density ($nb$) for unoxidised PDMS was calculated to be $0.06 \times 10^{-4}$ nm$^{-2}$. The silicon substrate had a $nb$ value of $2.11 \times 10^{-4}$ nm$^{-2}$. The inset figure depicts the profile of the scattering length density as a function of depth ($z$). The inset figure shows a very tiny step in $nb$ at $z = 0$. PDMS was thus almost indistinguishable from air. The smooth character of the log $R$–$Q$ curve indicates that the spin-coated PDMS layer was of uniform composition along the layer depth ($z$) direction.

The samples exposed to RF oxygen plasma showed small but distinct oscillations in the reflectivity as a function of $Q$ (Fig. 6b–f). The oscillations characterised a discrete layer with a different scattering length density (i.e. a different chemical composition) than of unoxidised PDMS, that appeared in the samples after plasma treatment. The spacing ($\Delta Q$) between successive peaks in the ripple can be used to estimate the thickness ($d$) of this layer: $d \approx 2\pi/\Delta Q$. The thickness of the layer was of the order of 130–160 nm and it can thus be concluded that the ripple is due to interference between air/oxidised PDMS and oxidised PDMS/silicone interfaces. The continuous lines shown in Fig. 6b–f represent the fitted reflectivity calculated using an asymmetric error function for the scattering length density profile at the interfaces. There are two possible interpretations: (a) the PDMS layer could have been uniformly "transformed" over its full thickness. Fig. 6g shows that the calculated log $R$–$Q$ curve based on this assumption ($nb = 1.33 \times 10^{-4}$ nm$^{-2}$) very clearly deviates from the experimental data for the specimen immediately after plasma exposure (180 s). (b) Alternatively, the sample could consist of an oxidised top layer with a rough interface with unoxidised PDMS in contact with the silicon wafer. Fig. 6h shows

Table 1
Fitted parameters from the neutron reflectometry measurements

| Plasma exposure time (s)/ ageing time (h) | Layer | *nb* ($nm^{-2}$) | Thickness[a] (nm) | Roughness of interface[a] (nm) |
|---|---|---|---|---|
| 80/144 | Oxidised | $1.21 \times 10^{-4}$ | 157 ± 2 | 10 ± 2[b] |
| | Unoxidised | $0.06 \times 10^{-4}$ | 90 ± 3 | 46 ± 2[c] |
| 80/288 | Oxidised | $1.27 \times 10^{-4}$ | 158 ± 3 | 10 ± 2[b] |
| | Unoxidised | $0.06 \times 10^{-4}$ | 92 ± 3 | 38 ± 2[c] |
| 180/0 | Oxidised | $1.33 \times 10^{-4}$ | 126 ± 3 | 14 ± 2[b] |
| | Unoxidised | $0.06 \times 10^{-4}$ | 80 ± 3 | 36 ± 2[c] |
| 180/144 | Oxidised | $1.33 \times 10^{-4}$ | 131 ± 3 | 14 ± 2[b] |
| | Unoxidised | $0.06 \times 10^{-4}$ | 85 ± 3 | 46 ± 2[c] |
| 180/288 | Oxidised | $2.11 \times 10^{-4}$ | 127 ± 3 | 18 ± 2[b] |
| | Unoxidised | $0.06 \times 10^{-4}$ | 82 ± 2 | 64 ± 2[c] |

[a] Optimum value ± accuracy.
[b] Roughness of interface between air and oxidised layer.
[c] Roughness of interface between oxidised and unoxidised layers.

the log *R*–*Q* data for a specimen immediately after plasma exposure (180 s) together with data obtained by using non-optimum parameter values for the thickness of the oxidised layer; 110 and 160 nm compared to the optimum 126 nm (Fig. 6d). The separation between the peaks remained essentially the same as in the case of using optimum thickness and roughness parameter values but the peaks were shifted along the *Q* axis giving rise to an overall poor fit. The neutron reflectometry data for specimens treated with RF oxygen plasma is summarised in Table 1. The roughness values presented in Table 1 correspond to the minimum values required to erase all evidence of an interface between oxidised and unoxidised PDMS from the calculated reflectivity. The actual width of this interlayer may well be larger. The uncertainties listed in Table 1 for the fitted parameters (layer thickness and interface roughness) were obtained by manually varying the parameters until the fit began to deviate significantly. A total thickness of the spin-coated layer of 200 nm was used as a fixed start parameter. The sensitivity of the final fits to the total thickness was in the order of 30 nm.

After RF oxygen plasma exposure for 80 s, the scattering length density of the oxidised top layer remained essentially constant at $1.21 \times 10^{-4}$ and $1.27 \times 10^{-4}$ $nm^{-2}$ after 144 and 288 h of ageing in air, respectively. After plasma treatment for 180 s, the scattering length density for the treated layer increased with increasing ageing time after the plasma treatment, from $1.33 \times 10^{-4}$ $nm^{-2}$ immediately after and 144 h after the oxygen-plasma exposure to $2.11 \times 10^{-4}$ $nm^{-2}$ after 288 h. The latter value is high compared to the aforementioned values. This result could, however, be consistent with additional reactions, such as condensation of silanol groups forming Si–O–Si bridges [27]. The constancy of the critical angle on storage after oxygen-plasma treatment indicated that the transport of low molar PDMS did not change the composition of the oxidised layer. It is important to emphasise that possible transport of low molar mass PDMS to the surface, forming a liquid PDMS top layer on the oxidised layer cannot be detected by neutron reflectometry, due to the low scattering length density of PDMS.

By calculating scattering length densities for different chemical compositions of the repeating unit, replacing the methyl groups by oxygen-containing species, the average composition of the formed species was assessed. The chemical structures and their scattering length densities are shown in Table 2. The scattering length densities of unoxidised PDMS and $SiO_2$ were calculated using the following densities: 967 kg $m^{-3}$ (PDMS) and 2660 kg $m^{-3}$ ($SiO_2$) [28]. The (*nb*) values of three other oxidised PDMS structures shown in Table 2 are based on density values calculated by the group contribution method proposed by

Table 2
Calculated scattering length densities for different repeating units

| Structure of repeating unit | Scattering length *nb* ($nm^{-2}$) |
|---|---|
| $-Si(CH_3)_2O-$ | $0.06 \times 10^{-4}$ |
| $-Si(CH_2OH)_2O-$ | $0.95 \times 10^{-4}$ |
| $-Si(CH_3,O)O-$ | $1.15 \times 10^{-4}$ |
| $-Si(OH)_2O-$ | $1.85 \times 10^{-4}$ |
| $-SiO_2-$ | $3.80 \times 10^{-4}$ |

Table 3
Elemental composition (at.%) by XPS of specimens exposed to MW oxygen plasma

| Plasma exposure time (s)/ ageing time (h) | Si | C | O |
|---|---|---|---|
| 0/– | 23.0 | 52.6 | 24.4 |
| 30/260 | 21.2 | 45.0 | 29.8 |
| 80/260 | 21.7 | 46.9 | 31.4 |
| 180/260 | 24.7 | 32.9 | 42.4 |

van Krevelen [29]. The calculated van der Waals densities (molar mass/van der Waals molar volume) for PDMS and $SiO_2$ were larger than the experimental densities. The difference between the two densities was believed to be due to free volume and it was assumed that the fractional free volume changed with the specific van der Waals volume in a linear manner from 36% for unoxidised PDMS to 3.2% for $SiO_2$. The calculated densities for $-Si(CH_2OH)_2-O-$, $-Si(CH_3,O)-O-$ and $-Si(OH)_2-O-$ became 1380, 1400 and 1700 kg $m^{-3}$, respectively.

The structures presented in Table 2 are based on reported data of the chemical changes in PDMS exposed to oxygen plasma from the literature: formation of silanol groups and reactions leading to the formation of crosslinks [10,23,27,30]. It may be assumed that the number of repeating units of the oxidised layer remained unchanged. Replacement of all methyl groups by hydroxyl groups yields a polymer with a scattering length density of $1.85 \times 10^{-4}$ $nm^{-2}$ (Table 2). A polymer with the hydroxyl groups bonded to the carbon atoms shows a (*nb*) value close to $0.95 \times 10^{-4}$ $nm^{-2}$. These calculated values are in the same range as the experimentally obtained values. Complete removal of all carbon and hydrogen atoms yields a polymer consisting only of silicon and oxygen with a scattering length density of $3.8 \times 10^{-4}$ $nm^{-2}$, which is higher than the obtained experimental values, $1.21–1.33 \times 10^{-4}$ $nm^{-2}$. If it is assumed that all the plasma-conversion products are $SiO_2$, the measured (*nb*) implies ~30% conversion of PDMS to $SiO_2$. XPS data assessing the structure of the top 10 nm presented in Section 3.6 suggested a mixture of species: $-Si(CH_3)_2-O-$ (59%), $-Si(O,CH_3)-O-$ (23%), and $SiO_2$ (18%). The percentage values given between brackets are molar contents for a specimen first exposed to 180 s of oxygen plasma and then aged for 260 h in dry air. The calculated (*nb*) value for this mixture of species using the values displayed in Table 2 amounted to $1.0–1.2 \times 10^{-4}$ $nm^{-2}$, which is in the same range as the experimental data obtained ($1.21–1.33 \times 10^{-4}$ $nm^{-2}$.) It is obvious that the surface is "contaminated" by diffusing low molar mass PDMS species and the virgin oxidised layer should contain more $SiO_x$. In a previous report [11], the structure of specimens exposed to corona discharges was assessed by XPS after removal of the extractable species. The calculated (*nb*) value using these data is $1.6–2.0 \times 10^{-4}$ $nm^{-2}$, which is 20–50% higher than the experimental data. It may thus be that the oxidised layer as it is revealed by neutron reflectometry is not of uniform composition.

### 3.4. Neutron reflectometry: thickness of oxidised surface layer

The thickness of the chemically modified layer decreased with increasing oxygen-plasma exposure time, from 157–158 nm after 80 s exposure to 126–131 nm after 180 s exposure (Table 1). The accuracy in these fitted parameters is almost an order of magnitude higher than the obtained difference in oxidised layer thickness between specimens exposed to 80 and 180 s (Table 1).

It is generally accepted that during exposure to an RF oxygen plasma, reactions at the immediate surface are due to recombination of both direct and radiative energy transfer whereas the subsurface reactions are dominated by radiative energy transfer by the ultraviolet (UV) component of the plasma [9]. The characteristic depth of penetration of UV usually does not exceed a few hundred nanometres [31,32], which is of the same order of magnitude as the calculated thickness of the oxidised layer (Table 1). The change in chemical composition (revealed by neutron reflectometry and XPS) due to oxidation caused a densification of the surface material. The appearance of surface cracks in heavily oxidised samples further supports the idea of a volume decrease of the surface material (Fig. 5). The decrease in the thickness of the oxidised layer may thus well be an effect caused by a decrease in specific volume of the oxidised material.

Owen and Smith [10] suggested, based on data obtained by XPS, that the thickness of the silica-like layer of plasma-treated PDMS was typically 10 nm, which is an order of magnitude smaller than the values reported here from neutron reflectometry. The magnitude difference in the measured thickness of silica-like layer may be due to differences in the plasma exposures used, and/or due to that the different analytical methods used, assess the oxidised layer differently.

### 3.5. Neutron reflectometry: interfaces and interfacial roughness

The absence of any reflectivity fringes other than those of the 200 nm total film thickness allowed only an estimation of the minimum interfacial roughness between oxidised and unoxidised PDMS layers. The roughness data shown in Table 1 refer to the two interfaces: i.e. the interface between air and the oxidised layer—*interface 1* or to the interface between the oxidised and unoxidised layers—*interface 2* (Fig. 1). The roughness of interface 1 remained relatively unchanged after treatment for 80 and 180 s, between 10–18 nm, and a prolonged storage after the plasma treatment had no effect on the roughness. AFM data presented in another part of this paper confirmed the invariant surface roughness. The roughness of interface 2 also remained relatively unchanged with increasing storage time for the samples exposed to 80 s of RF oxygen plasma. For the sample exposed to RF oxygen-plasma for 180 s, the interfacial roughness increased from 36 to 64 nm during 288 h of ageing in dry air after the oxygen-plasma exposure. This could be an indication of migration of low molar mass PDMS from the unoxidised layer towards the oxidised layer.

### 3.6. X-ray photoelectron spectroscopy

Data for the elemental composition of the 8–10 nm top layer obtained by XPS of the spin-coated specimens are

Table 4
Results of curve resolution of the Si 2p peak of specimens exposed to MW oxygen plasma

| Exposure time (s)/ ageing time (h) | $-Si(CH_3)_2-O-$ (102.1 eV) (%) | $-Si(CH_3,O)-O-$ (102.8 eV) (%) | $SiO_2$ (103.4 eV) (%) |
|---|---|---|---|
| 30/260 | 79 | 17 | 4 |
| 80/260 | 68 | 21 | 11 |
| 180/260 | 59 | 23 | 18 |

presented in Table 3. It should be noted that the XPS data were taken after 260 h of ageing in dry air and the plasma-exposed specimens had recovered a significant part of their original hydrophobicity (see Fig. 4). The unexposed specimen showed an atomic composition (23.0% Si, 52.6% C and 24.4% O) similar to the theoretical atomic composition of PDMS: 25% Si, 50% C and 25% O. Exposure to the MW oxygen plasma increased the oxygen content from the original 24.4 to 42.4% after 180 s of plasma treatment, whereas the carbon content decreased from the original 52.6 to 32.9 at.% after 180 s of plasma treatment. The silicon content remained essentially constant. These results are in accordance with earlier data for PDMS exposed to oxygen plasma [3,10]. Specimens exposed to corona discharges followed by solvent extraction showed significantly higher oxygen contents, maximum ~56 at.%, and also much lower carbon contents, minimum ~14 at.% [11]. The extractable species present in the MW plasma-exposed specimens reported here evidently migrated to the surface and lowered the oxygen content and increased the carbon content.

Fig. 7 shows the high-resolution spectra of the Si 2p peak for unexposed and MW oxygen-plasma-exposed PDMS. Unexposed PDMS displayed only one peak at 102.1 eV. The MW oxygen-plasma-treated samples showed a broadening of the Si 2p peak and a shift towards higher binding energies indicating a change in the chemical state of the silicon atoms.

The complex Si 2p peaks of the plasma-treated samples were resolved into three components in accordance with Alexander et al. [33]: Si bound to two oxygens at 102.1 eV, Si bound to three oxygens at 102.8 eV and Si bound to four oxygens ($SiO_2$) at 103.4 eV. The peak positions were kept at 102.1, 102.8 and 103.4 eV with an accuracy of ±0.1 eV and both the width parameters and the amplitudes of the three gaussian peaks were adjusted in fitting the model to the experimental data. The full width at half maximum (FWHM) was kept below 1.5 eV. Essentially only the amplitudes of the different peaks varied with plasma exposure time. Particularly, the $SiO_2$ content increased with increasing plasma exposure time (Table 4). The elemental compositions calculated from the proportions of the different species as obtained from the resolution of Si 2p peaks were in accordance with the elemental compositions as obtained from the survey spectra. Again, it should be noted that the spectra displayed in Fig. 7 are from specimens that had been aged in dry air for 260 h. Migration of low molar mass PDMS, which was confirmed by the change in elemental composition with ageing time (Table 5), caused a progressive reduction in the relative amount of $SiO_x$. Specimens prepared by solvent extraction following corona treatment showed considerably higher $SiO_x$ contents [11].

Table 5
Elemental composition (at.%) by XPS of specimens exposed to MW oxygen plasma for 80 s and after different times of storage in dry air at room temperature

| Ageing time (h) | Si | C | O |
|---|---|---|---|
| 3 | 20.3 | 35.2 | 44.4 |
| 93 | 21.2 | 43.3 | 35.5 |
| 260 | 21.7 | 46.9 | 31.4 |

Table 5 shows the elemental composition of a series of specimens, all exposed to the same MW oxygen plasma dose and then aged for different times in dry air at room temperature. The decrease in oxygen content and increase in carbon content with increasing ageing time suggests that migration of PDMS, supposedly of low molar mass, occurred. Thus, the oxidised top layer was gradually coated with a thin liquid film of low molar mass PDMS.

### 3.7. The Wilhelmy balance: hydrophobicity and surface mobility

The force–immersion depth recording for unexposed PDMS is shown in Fig. 2. An important feature of the behaviour of this specimen is the absence of a step in the hysteresis loop when the wetting line is moved from a

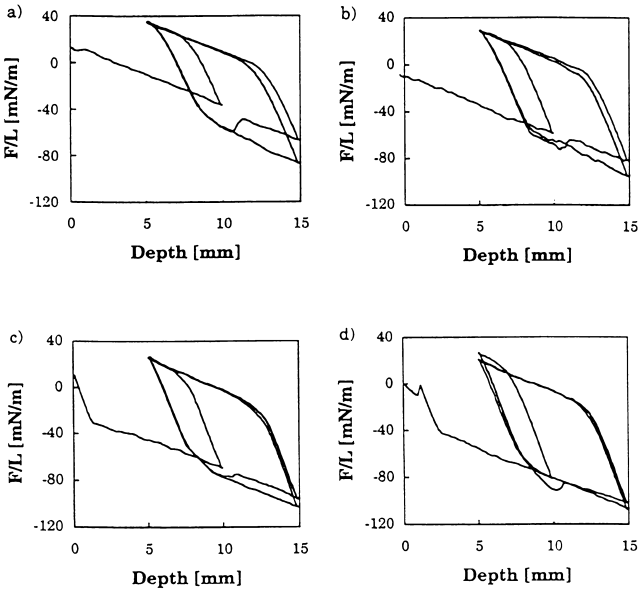


Fig. 8. The measured force as a function of immersion depth recorded for specimens exposed to RF oxygen plasma for 30 s after different ageing times at 25°C in air: (a) 0.8 h.; (b) 24 h; (c) 144 h; (d) 288 h.

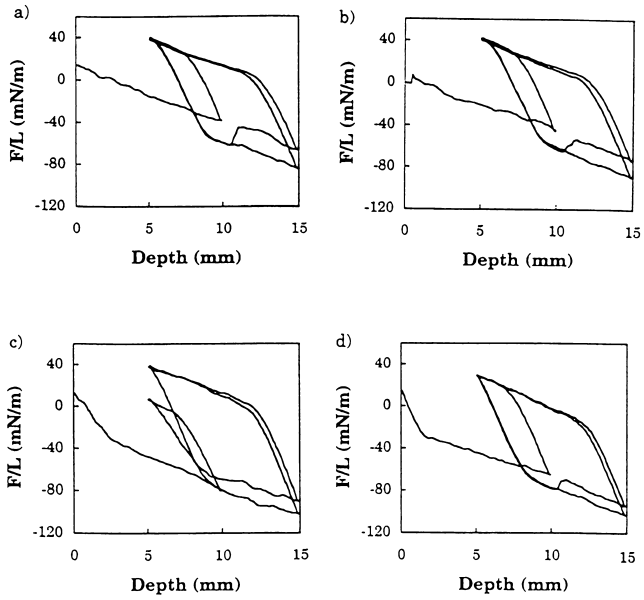


Fig. 9. The measured force as a function of immersion depth recorded for specimens exposed to RF oxygen plasma for 80 s after different ageing times at 25°C in air: (a) 0.25 h; (b) 24 h; (c) 144 h; (d) 288 h.

pre-wetted area to a dry one on the specimen. A large step indicates large differences between high and low surface energy regions of the polymer surface [34] and the obtained data indicated that the differences in surface energy were small on the unexposed polymer. The high hysteresis is another characteristic of this specimen (Fig. 2). The amplitude of the loop, the hysteresis, is dependent on the short-range motions of segments close to the surface [35]. The large hysteresis thus demonstrated the high segmental mobility of the siloxane backbone in unexposed PDMS.

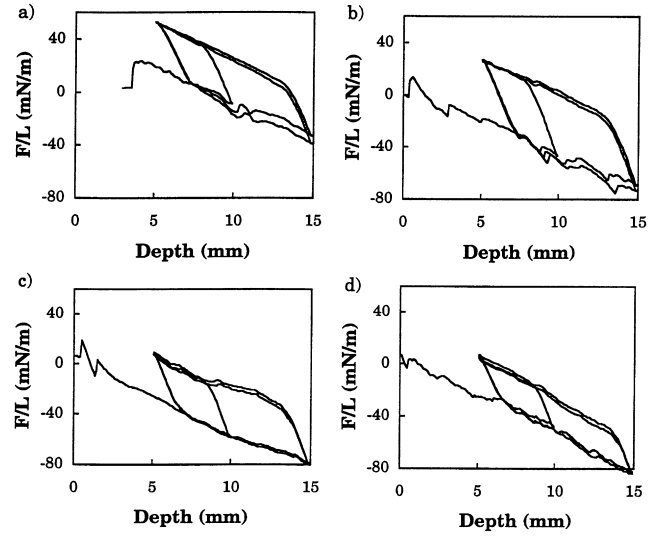


Fig. 10. The measured force as a function of immersion depth recorded for specimens exposed to RF oxygen plasma for 180 s after different storage times at 25°C in air: (a) 0.63 h; (b) 24 h; (c) 144 h; (d) 288 h.

The effects of RF oxygen-plasma exposure on the surface dynamics during 30, 80 and 180 s of exposure are shown in Figs. 8–10. The hysteresis loop amplitudes, of the specimens recorded directly after oxygen-plasma exposure, decreased with increasing exposure time. The same phenomenon has been reported by the sessile drop technique [11] for silicone rubbers exposed to corona discharges in dry air. The formation of a silica-like, more rigid structure induced by the oxygen plasma is expected to decrease the segmental mobility of the surface material and hence the hysteresis amplitude.

The specimen exposed to RF oxygen plasma for 30 and 80 s showed a decrease in step size and an increase in the hysteresis amplitude after storage in dry air. The migration of low molar mass PDMS to the surface, confirmed by the XPS data, covered the oxidised layer and caused a pronounced increase in the segmental mobility of the surface material. The specimen exposed to plasma for 180 s exhibited a smaller initial step and initially a very low hysteresis. This is probably due to the more extensive surface oxidation, compared to the specimen exposed for shorter times. For all the plasma-treated specimen, the loops moved towards lower values with increasing time, due to the hydrophobic recovery.

It was found that the specimens became more hydrophobic after the first immersion in water, i.e. during the second cycle. It is suggested on the basis of these results and on results from measurements using the Du Nouy ring method (the surface tension was reduced by ~10% after water immersion of the samples) that oxidised low molar mass PDMS or impurities are transferred to the water phase. The lowering of surface tension was also observed for unexposed PDMS.

## 4. Conclusions

Spin-coated films of silicone rubber were exposed to oxygen plasma for different periods of time. Specular neutron reflectivity and XPS showed that the RF oxygen-plasma treatment led to the formation of a smooth oxidised surface layer (thickness: 130–160 nm) containing a significant fraction of silicon bonded to three or four oxygen atoms ($SiO_x$). The oxidised layer became thinner on prolonged plasma exposure, indicating a decrease in specific volume due to a conversion of the organic polymer structure to inorganic $SiO_x$-rich structure. The formation of a $SiO_x$-containing layer with low segmental flexibility was confirmed by the small hysteresis in the Wilhelmy balance measurements. The similarity in the hydrophobic recovery kinetics, as assessed by contact angle measurements, of oxygen plasma treated specimens aged in different atmospheres (dry air, argon and vacuum) and XPS results showed that hydrophobic recovery was not due to contamination through adsorption from the atmosphere. Instead we propose that the recovery is due to migration of low molar

mass species to the surface. Scanning electron microscopy showed the presence of surface cracks in heavily oxidised specimens.

## Acknowledgements

The Swedish Research Council for Engineering Sciences (TFR; grant 285-95-606), ABB Corporate Research, Västerås and the Franz-Georg and Gull Liljeroths foundation are thanked for sponsorship. The experimental assistance of R. Gaston, M. Lewis, S. Mitchell and M. Miyama at the University of Missouri-Columbia, USA and B. Olander, Department of Polymer Technology, Royal Institute of Technology is gratefully acknowledged.

## References

[1] Gubanski SM, Vlastós AE. IEEE Trans Power Deliv 1990;5:1527.
[2] Kim SH, Cherney EA, Hackam R. IEEE Trans Electr Insul 1992;6:1065.
[3] Tóth A, Bertóti I, Blazsó M, Bánhegyi G, Bognar A, Szaplonczay X. J Appl Polym Sci 1994;52:1293.
[4] Kim SH, Cherney EA, Hackham R. Conf Records IEEE Inter Symp Electr Insul 1992:237.
[5] Chang JW, Gorur RS. IEEE Trans Dielectr Electr Insul 1994;1:1039.
[6] Gorur RS, Mishra J, Tay R, McAfee R. IEEE Trans Dielectr Electr Insul 1996;3:299.
[7] Eveaert EP, van der Mei HC, Busscher HJ. Polym Prepr 1995;36:89.
[8] Homma H, Kuroyagi T, Mirley CL, Ronzello J, Boggs SA. IEEE Int Symp Electr Insul 1996:279.
[9] Gerenser LJ. J Adhes Sci Technol 1993;7:1019.
[10] Owen MJ, Smith PJ. J Adhes Sci Technol 1994;8:1063.
[11] Hillborg H, Gedde UW. Polymer 1998;39:1991.
[12] Russell TP. Materials science reports, vol. 5. Amsterdam: Elsevier, 1990 p. 171.
[13] Sanchez IC. Physics of polymer surfaces and interfaces. London: Butterworth-Heinemann, 1992.
[14] Schubert DW, Stamm M. Europhys Lett 1996;35:419.
[15] Feng Y, Weiss RA, Karim A, Han CC, Ankner JF, Kaiser H, Peiffer DG. Macromolecules 1996;29:3918.
[16] Kaiser H, Hamacher K, Kulasekere R, Lee W-T, Ankner JF, DeFacio B, Miceli P, Worcester DL. Inverse Optics III—Soc Photo-Optic Instrum Engrs 1994;2241:78.
[17] Sears VF. Neutron News 1992;3:26.
[18] Klein AG, Werner SA. Rep Prog Phys 1983;46:259.
[19] Ankner JF, Majkrzak CF. Neutron optical devices and applications. In: Majkrzak CF, Wood JL, editors, SPIE Conference Proceedings, 1738, SPIE, Bellingham, WA, 1992, p. 260.
[20] Garbassi F, Morra M, Occhiello E. Polymer surfaces. New York: Wiley, 1994.
[21] Miyama M, Yang Y, Yasuda T, Okuno T, Yasuda HK. Submitted for publication.
[22] Adamson AW. Physical chemistry of surfaces. 2nd ed. New York: Interscience, 1967.
[23] Owen M, Gentle M, Orbeck T, Williams DE. In: Andrade JD, editor. Polymer surfaces dynamics, New York: Plenum Press, 1988.
[24] Fritz JL, Owen MJ. J Adhes 1995;54:33.
[25] Hillborg H, Karlsson S, Gedde UW. Manuscript.
[26] Gedde UW, Hellebuyck A, Hedenqvist M. Polym Engng Sci 1996;36:2077.
[27] Morra M, Occhiello E, Marola R, Garbassi F, Humphrey P, Johnson D. J Coll Interf Sci 1990;137:11.
[28] Weast RC, editor. Handbook of chemistry and physics 57th ed.. Cleveland, OH: CRC Press, 1976.
[29] van Krevelen DW. Properties of polymers. 3rd ed.. Amsterdam: Elsevier, 1990.
[30] Hollahan JR. J Appl Polym Sci 1970;14:2499.
[31] Skurat VE, Dorofeev YI. Angew Macromol Chem 1994;216:205.
[32] Vasilets VN, Nakamura K, Ogata S, Ikada Y. Polymer 1998;39:2875.
[33] Alexander MR, Short RD, Jones FR, Stollenwerk M, Michaeli W, Blomfeld CJ. Appl Surface Sci 1999;137:179.
[34] Chang JH, Claesson PM, Parker JL, Yasuda HK. Langmuir 1994;10:3887.
[35] Tretinnikov ON, Ikada Y. Langmuir 1994;10:1606.